

# Performance Optimization and Real-Time Security Monitoring for Single-Photon Quantum Key Distribution

Timm Kupko,<sup>1</sup> Martin v. Helversen,<sup>1</sup> Lucas Rickert,<sup>1</sup> Jan-Hindrik Schulze,<sup>1</sup> André Strittmatter,<sup>1,2</sup> Manuel Gschrey,<sup>1</sup> Sven Rodt,<sup>1</sup> Stephan Reitzenstein,<sup>1</sup> and Tobias Heindel<sup>1,\*</sup>

<sup>1</sup>*Institut für Festkörperphysik, Technische Universität Berlin, 10623 Berlin, Germany*

<sup>2</sup>*Present address: Institut für Experimentelle Physik,*

*Otto-von-Guericke Universität Magdeburg, 39106 Magdeburg, Germany*

Quantum light sources emitting triggered single photons or entangled photon pairs have the potential to boost the performance of quantum key distribution (QKD) systems. Proof-of-principle experiments affirmed these prospects, but further efforts are necessary to push this field beyond its current status. In this work, we show that temporal filtering of single-photon pulses enables a performance optimization of QKD systems implemented with realistic quantum light sources, both in experiment and simulations. To this end, we analyze the influence of temporal filtering of sub-Poissonian single-photon pulses on the expected secret key fraction, the quantum bit error ratio, and the tolerable channel losses. For this purpose, we developed a basic QKD testbed comprising a triggered solid-state single-photon source and a receiver module designed for four-state polarization coding via the BB84 protocol. Furthermore, we demonstrate real-time security monitoring by analyzing the photon statistics, in terms of  $g^{(2)}(0)$ , inside the quantum channel by correlating the photon flux recorded at the four ports of our receiver. Our findings are useful for the certification of QKD and can be applied and further extended for the optimization of various implementations of quantum communication based on sub-Poissonian quantum light sources, including device-independent schemes of QKD as well as quantum repeaters. Our work represents an important contribution towards the development of QKD-secured communication networks based on quantum light sources.

## INTRODUCTION

Cyber security and secure data communication in general developed as a challenge for our society as a whole [1]. The concepts gathered in the field of quantum communication [2–4] represent solutions to this challenge and enable information theoretical secure communication. Quantum key distribution (QKD) for instance enables the tap-proof encryption of data, by exploiting quantum properties of light [5, 6]. The respective quantum light sources ideally required for QKD, however, had been impossible to fabricate with sufficient brightness and quality for a long time. Most implementations of QKD are therefore still implemented with attenuated lasers, requiring so-called decoy-state protocols [7]. During the last decade, however, tremendous progress has been made in the fabrication of quantum light sources. Single-photon sources (SPSs) based on epitaxial semiconductor quantum dots (QDs) nowadays can be triggered at GHz clock rates under pulsed-optical [8] and -electrical [9, 10] excitation, feature high degrees of photon indistinguishability [11, 12], large photon extraction efficiencies [10, 13, 14], and to date achieve the highest single-photon purity in terms of  $g^{(2)}(0)$  compared to any other single-photon emitter [15, 16]. Despite this immense progress, only few proof-of-concept QKD experiments have been reported based on optically [17–22] and electrically [23, 24] operated single-photon sources. These experiments affirmed the potential sub-Poissonian light sources offer for QKD. To push the field of sub-

Poissonian QKD to a new level, however, further efforts need to be undertaken. In particular practical methods for the security analysis and certification as well as measures to improve the performance of QKD systems for a given quantum light source need to be developed. While Waks et al. discussed security aspects of QKD with sub-Poissonian light sources from a theoretical viewpoint [25], experimental studies on this important topic are still missing.

In this work, we perform a detailed analysis on the influence of temporal filtering of single-photon pulses on the performance of QKD systems implemented with sub-Poissonian light sources. For this purpose we set up a basic QKD testbed comprising a QD-based SPS and a receiver module designed for four-state polarization coding via the BB84 protocol. Using this Bob module in combination with our SPS, we determine the sifted key fraction, the quantum bit error ratio (QBER) caused by the receiver, and the  $g^{(2)}(0)$  of the single-photon pulses inside the quantum channel, to finally extract the secure key rate expected in full implementations of QKD. As the temporal filtering of single-photon pulses differently affects these parameters, a performance optimization of QKD systems implemented with quantum light source is possible. We show that optimal performance for a given SPS can be achieved by carefully setting Bob's acceptance time windows, depending on the pulse shape and noise level. This can be either used to maximize the secure key rate for a given channel loss or to extend the maximally tolerable loss, i.e. the achievable communication distance. In addition, we demonstrate real-time se-

curity monitoring by analyzing the suppression of multi-photon emission events, i.e.  $g^{(2)}(0)$  of the single-photon pulses inside the quantum channel during key generation. Finally we generalize our findings by employing simulations with synthetic pulse shapes, providing predictions for different SPSs and detectors. We consider the results presented in this work an important contribution towards the development of QKD-secured communication networks based on quantum light sources. Importantly, our approach can be easily applied and further extended for the optimization of any implementation of quantum communication based on sub-Poissonian quantum light sources.

## RESULTS

### QKD testbed

The QKD testbed used for our experiments is illustrated in Fig. 1 (a). On transmitter side, Alice is represented by a triggered SPS, comprising a single pre-selected QD embedded in a deterministically fabricated microlens [26] providing enhanced photon collection efficiency (see Methods for details). As depicted in Fig. 1 (b) this device emits single photons at an emission wavelength of 918 nm with low multi-photon emission probability reflected in an antibunching of  $g^{(2)}(0) = 0.089 \pm 0.002$ . The polarization state of the emitted photons is set by a high-extinction-ratio linear-film polarizer and a lambda-half waveplate, respectively, preparing single-photon pulses in horizontal (H), vertical (V), diagonal (D), and antidiagonal (A) polarization. On receiver side, Bob comprises a four-state polarization analyzer with passive basis choice. Single-photon counting modules based on silicon avalanche photon diodes, time tagging electronics and a custom made control software is used for polarization-resolved single-photon detection, data acquisition, and postprocessing. The Bob module is integrated into a portable 19-inch rackbox presented in Fig. 1 (c) (see Methods for details). In the following, we investigate the performance of this QKD testbed assuming an implementation of the BB84 protocol by analyzing the achievable QBER, single-photon purity  $g^{(2)}(0)$  and secret key rate.

First we investigate the limit our Bob module introduces to the total QBER expected in a full implementation. For this purpose, we record the photon arrival time distribution at the four detection channels of Bob for all four possible input polarizations of the SPS. The corresponding experimental data are shown in Fig. 1 (d) in a matrix representation. Ideally, for a given input polarization (e.g. H) of one basis (H-V), one would expect only detection events in the respective channel at Bob's side (H), while the channel with orthogonal polarization (V) should be empty. Detection events in the other basis (D-

A) should be equally distributed, due to the statistically random projection of the photons polarization. From the measured matrix in Fig. 1 (d) this appears to be well reproduced in the experiment. A closer look in Fig. 1 (d) (right panel), however, reveals the presence of erroneous detection events, by displaying the arrival time probability distributions of both polarizations of the target basis. In this representation, contributions of noise and optical imperfections can already be qualitatively distinguished. Correlated events in the wrong channel originate from state discrimination imperfections caused by optical imperfections of Bob (e.g. finite extinction ratios of polarizing beamsplitters and retardance deviations of waveplate), while uncorrelated background events stem from detector dark counts. The resulting  $\text{QBER}_{\text{Bob}}$  reads

$$\text{QBER}_{\text{Bob}} = \underbrace{\frac{qp_{\text{signal}}}{p_{\text{click}}}}_{\text{optical imperfections}} + \underbrace{\frac{p_{\text{dc}}/2}{p_{\text{click}}}}_{\text{dark counts}}, \quad (1)$$

where  $q$  denotes the error contributions due to Bob's optical imperfections,  $p_{\text{signal}}$  is the probability to observe a signal event,  $p_{\text{dc}}$  the probability for a dark count event, and  $p_{\text{click}}$  the overall probability for a click [25].

### Performance optimization via temporal filtering

In the following, we analyze the impact of the temporal filtering of the raw sifted key on the performance of our single-photon QKD testbed. Experimentally, the error contribution in the H-channel is calculated via  $\text{QBER}_{\text{Bob}}^{\text{H}}(\Delta t, t_c) = N_V/(N_{\text{H}} + N_V)$ , where  $N_{\text{H}}$  and  $N_V$  denote the number of clicks in H and V polarization, respectively, detected within an acceptance time window of width  $\Delta t$  centered at time  $t_c$ . Restricting the acceptance time window, the signal-to-noise-ratio can be enhanced, as noise due to detector dark counts can be filtered effectively [24, 27]. Fig. 2 (a) exemplarily illustrates the measured photon arrival time probability distributions at both detectors of the H-V basis (H-polarized single-photon input) together with an acceptance time window  $\Delta t = 2.5 \text{ ns}$  centered at the pulse maximum ( $t_c = 6.25 \text{ ns}$ ). Evaluating  $\text{QBER}_{\text{Bob}}^{\text{H}}(\Delta t, t_c)$  by applying a temporal filter to the recorded timetags, the QBER and the fraction  $F$  of the sifted and filtered photon detection events can be extracted as a function of  $\Delta t$  (see Fig. 2 (b)). Restricting the acceptance time window  $\Delta t$  leads first of all to a reduction of the sifted key, as portions of the overall signal are discarded. At the same time the contribution of the detector dark counts is reduced, leading to a decrease of  $\text{QBER}_{\text{H}}$  towards small  $\Delta t$ . At  $\Delta t = 1.7 \text{ ns}$  a local minimum with  $\text{QBER}_{\text{H}} = 0.45\%$  limited by optical imperfections inside the receiver is observed. Note, that the global minimum in  $\text{QBER}_{\text{H}}$  at  $\Delta t = 0.05 \text{ ns}$  is not taken into account, due to the vanishing sifted key. The remaining three channels of the

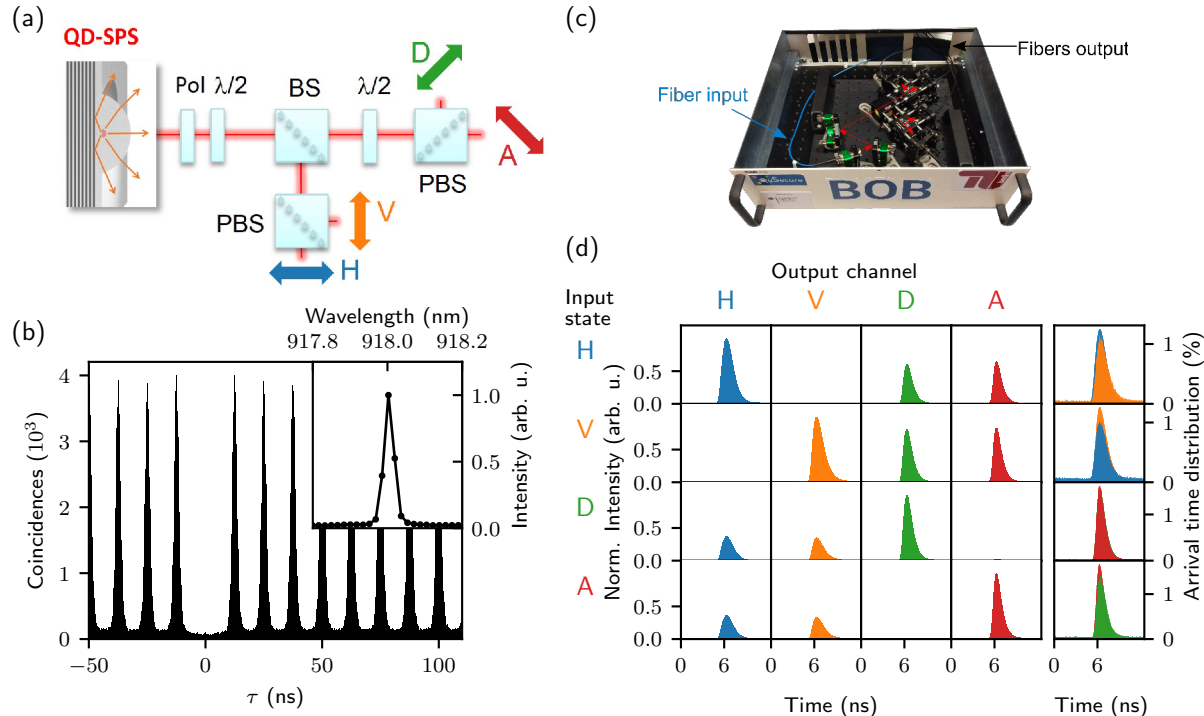


FIG. 1. BB84-QKD testbed using a triggered solid-state single-photon source (SPS) and polarization coding. (a) The transmitter (Alice) sends single-photon pulses with fixed polarization (H, V, D, and A) to the receiver module (Bob), comprising a four-state polarization analyzer. (b) Photon-autocorrelation measurement of the emission of the optically triggered SPS. Inset: Emission spectrum of the SPS, comprising a pre-selected quantum dot embedded in a photonic microlens. (c) Picture of the Bob module integrated in a 19-inch rackbox. (d) Measured photon arrival time distributions at the four detection channels of Bob for single-photon input-polarizations of H, V, D, and A. Measurement data are normalized to the maximum of the respective input state. The right panel shows the two data sets for a given input polarization basis (e.g. HH and HV) for each input state normalized to the photon arrival probability distributions, revealing erroneous detection events due to optical imperfections in Bob.

Bob module show similar behavior (see Supplementary Note 1). The temporal filtering, however, does not only affect the QBER and the sifted key fraction. The photon statistics of the quantum light source needs to be taken into account for a security analysis as well. The multi-photon probability  $p_m$  inside the quantum channel is governed by  $g^{(2)}(0)$  via

$$p_m \leq \frac{\mu^2 g^{(2)}(0)}{2}. \quad (2)$$

For the antibunching relevant for QKD, only the fraction of the detection events has to be taken into account which are used for secret key distillation in the end. Therefore we evaluate the photon-autocorrelation  $g^{(2)}(\tau)$  from the raw recorded timetags of all four detection channels after applying the temporal filter to the data (see Fig. 2(c)). The corresponding  $g_{\Delta t}^{(2)}(0)$  extracted from the temporally filtered timetags (see Methods) is displayed in Fig. 2(d) as a function of  $\Delta t$ . Narrowing the temporal filter, the antibunching improves from  $0.103 \pm 0.009$  at  $\Delta t = 12.50$  ns to  $0.016 \pm 0.007$  at  $\Delta t = 1.1$  ns. Note, that this approach has to be well dis-

tinguished from most other reports, where postselected values of  $g^{(2)}(0)$  are generated based on the cutting of  $g^{(2)}(\tau)$  after performing the correlation measurement using all photon detection events. In contrast, our routine only considers photon detection events used for secure key distillation in the end, which is more precise. In addition, background subtraction of coincidences due to detector dark counts, residual laser emission [29] or the sample emission other than the quantum emitter itself [30–32] is often used to explain the non-ideal  $g^{(2)}(0)$ . Clearly such approaches are not meaningful for implementations of QKD, since in general detection events arising from noise can not be differentiated from the signal ones. Still these considerations can be useful to underline the potential a given quantum light source offers.

Exploiting temporal filtering as discussed above, the overall performance of a QKD implementation based on single-photon sources can be optimized as we will demonstrate in the following. For this purpose, a trade-off needs to be found between low QBER and low

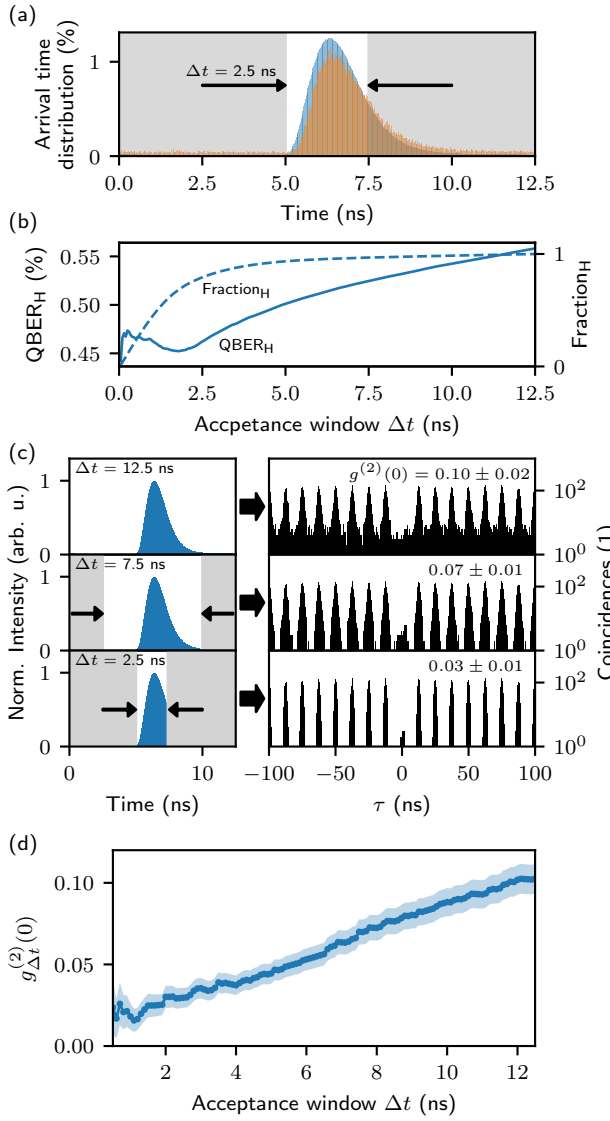


FIG. 2. The effect of temporal filtering on key parameters of QKD (exemplary shown for H input polarization). (a) Photon arrival time probability distributions of H-photon (blue) and V-photon (orange) detected in the H-channel. Applying temporal filtering, noise due to detector dark counts can be reduced. (b) QBER and sifted key fraction  $F$  as a function of the acceptance time window width  $\Delta t$  for fixed window center  $t_c$ . (c) Impact of the temporal filtering on the  $g^{(2)}(0)$  of our single-photon source. Each correlation histogram  $g^{(2)}(\tau)$  is calculated from the raw recorded timetags of all four detection channels after applying the temporal filter to the data for an evaluation time of 180 s. This evaluation time corresponds to the first data point in Fig. 4 (b). (d)  $g^{(2)}(0)$  as a function of  $\Delta t$ .

$g^{(2)}(0)$  on the one hand, and high sifted key fractions on the other hand. In addition, a symmetric temporal filter as chosen above is not sufficient in general, due to the asymmetry in the photon arrival time distribution of

the single-photon pulses. To this end, we perform a two-dimensional (2D) analysis by varying the temporal width  $\Delta t$  and the center  $t_c$  of the acceptance time window. The 2D analysis is performed for the QBER<sub>Bob</sub><sup>H</sup>( $\Delta t, t_c$ ), the sifted fraction  $F_{Bob}^H(\Delta t, t_c)$ , and the antibunching  $g^{(2)}(0, \Delta t, t_c)$  (see Supplementary Note 2 and 3). From these quantities, we finally extract the normalized secret key rate  $S(\Delta t, t_c)$  expected in a full implementation of BB84 QKD according to [17]

$$R = \frac{p_{\text{click}}}{2} (\beta \tau(e) - f(e)h(e)) . \quad (3)$$

Here, the factor 1/2 stems from the sifting procedure,  $p_{\text{click}}$  is the click-rate on the detectors,  $e$  the QBER,  $\beta$  the fraction of the detection events caused by single photons,  $\tau(e)$  the compression function accounting for Eve's possible attacks,  $h(e)$  the binary Shannon-entropy, and  $f(e)$  the error correction efficiency [25]. The expected back-to-back secret key rate calculated from Eq. 3 is presented in Fig. 3 (a). A small  $\Delta t$  leads to a small QBER but also

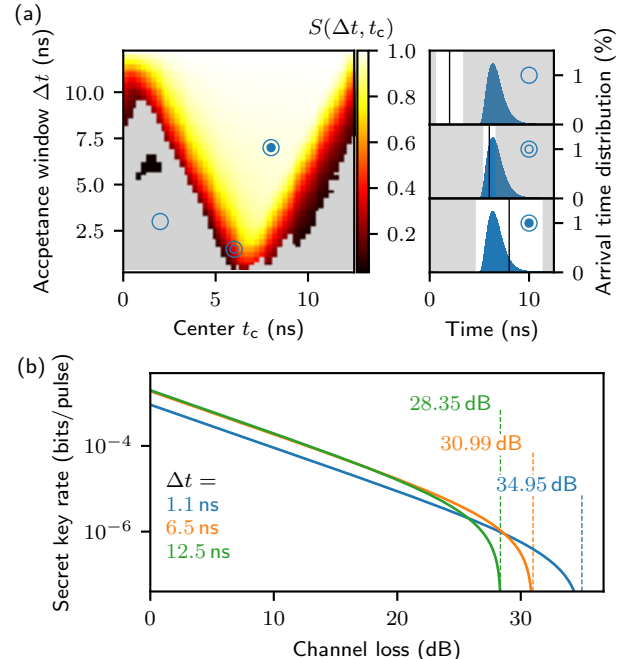


FIG. 3. Optimization of single-photon QKD exploiting temporal filtering of realistic quantum light sources. (a) Expected secret key rate fraction  $S(\Delta t, t_c)$  as a function of the temporal width  $\Delta t$  and the center  $t_c$  of the acceptance time window. For the analysis the QBER, the sifted key fraction and the  $g^{(2)}(0)$  were considered in a two-dimensional parameter space ( $\Delta t, t_c$ ) (see Supplementary Note 3). Grey areas indicate parameters where no secret key can be extracted. (b) Rate-loss diagram considering our experimental data from Fig. 2 (d) for different values of  $\Delta t$ . Choosing optimized settings for the acceptance time window, the tolerable loss inside the quantum channel can be enhanced by 23% in case of our SPS.

to a small sifted fraction. An acceptance window within

a region governed by noise does not allow for a secret key distribution at all. The optimal value for our measurement does only need to discard a small part of the signal. Depending on the length of the single-photon pulses and the detector noise level, however, temporal filtering can have crucial impact on the resulting back-to-back secure key, as demonstrated in simulations discussed further below.

The secure communication distance achievable with a given QKD system is of superior importance. Based on the secret key analysis performed in Fig. 3(a), we calculated the rate-loss dependencies accounting for our experimental conditions (see Methods). Fig. 3(b) illustrates the expected secret key per pulse as a function of the losses inside the quantum channel for different temporal filters. In the low-loss regime ( $< 20$  dB) optimum back-to-back performance is achieved for our SPS by using the full acceptance time window ( $\Delta t = 12.5$  ns), as already discussed above. The maximal tolerable loss, however, is limited to 28.35 dB in this case. Applying a temporal filter, the achievable maximal tolerable loss inside the quantum channel can be enhanced to almost 35 dB for an optimized filter setting ( $\Delta t = 1.1$  ns), which corresponds to a QKD range extension of 23%. This transmission range extension is possible due to the improvement in signal-to-noise ratio and the reduced multi-photon probability  $g^{(2)}(0)$  resulting from the temporal filtering (see Supplementary Note 4). Assuming a single-photon source of similar performance with an emission wavelength of 1310 nm and 1550 nm, respectively, extensions for the secure communication distance by 21.3 km (to a distance of 112.8 km) and 38.9 km (to a distance of 205.6 km) are expected, for state-of-the-art single-mode fiber (Corning SMF28-ULL) with 0.31 dB/km and 0.17 dB/km at 1310 nm and 1550 nm, respectively.

Importantly, the optimization routine presented above can be adapted and extended for most other applications in quantum communication employing realistic quantum light sources, including future implementations of multi-user quantum networks based on measurement device-independent QKD [33] or multi-dimensional memory-based quantum repeaters [34].

### Real-time photon statistics monitoring

In future QKD-secured networks implemented with quantum light sources,  $g^{(2)}(0)$  inside the quantum channel needs to be monitored in real time to enable secret key distillation. Moreover, any temporal filtering applied to the detected photons on Bob's side needs to be applied to the photon statistics as well. So far, in most reports on single-photon QKD, the  $g^{(2)}(0)$  used for the security analysis has been measured separately from the key transmission, using for instance a Hanbury-Brown and Twiss setup on Alice's side. Applying our approach for the op-

timization via temporal filtering presented above, we are able to monitor  $g^{(2)}(0)$  in real-time and for each block used for secret key distillation. For this purpose, we conducted a proof-of-principle experiment by recording time tags over a period of 90 minutes with fixed input polarization  $H$  of our SPS. The photon statistics  $g^{(2)}(\tau)$  are evaluated every 180 s (non-overlapping blocks) by correlating the time tags of all four detection channels of Bob. The resulting time traces for  $g^{(2)}(0)$  and the sifted key are presented in Fig. 4.

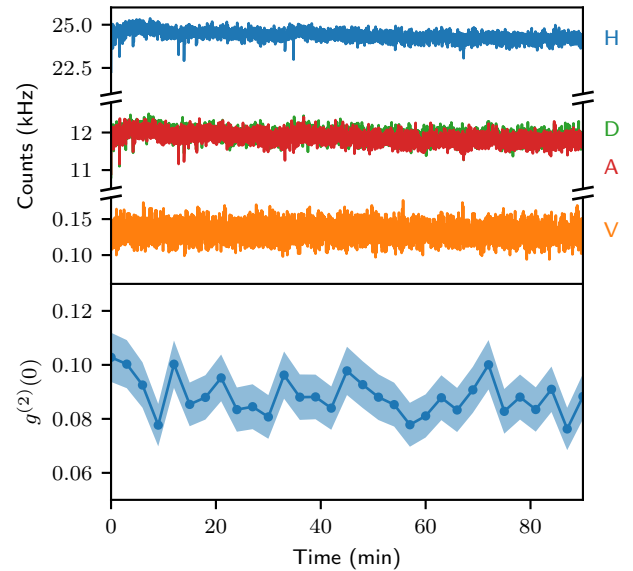


FIG. 4. Real-time security monitoring for single-photon QKD. (a) Clicks recorded in all four detection channels of Bob for  $H$ -polarized single-photons as input. (b) Antibunching  $g^{(2)}(0)$  of our SPS evaluated via correlating the time tags of all four detection channels in non-overlapping blocks of 180 s length.

Via the monitoring of  $g^{(2)}(0)$ , the quantum optical properties of our SPS can be tested continuously during secret key distillation. This approach, which has previously been used only for coherent and bunched light sources [35, 36], is able to reveal changes in the transceiver module or eavesdropping attacks inducing changes in the photon statistics.

### Simulations

To extend the scope of our approach for the performance optimization of single-photon QKD systems beyond the specific properties of our testbed, we additionally performed simulations on the secret key fraction expected for different single-photon sources and detectors. For this purpose, we modeled the photon arrival time distributions of the single-photon pulses with a synthetic pulse shape and varied the decay time constant as well as the noise level (see Methods). For the sake of clarity,

we limit ourselves to four regimes: (1) Low noise and short lifetime, (2) high noise and short lifetime, (3) low noise and long lifetime, and (4) high noise and long lifetime, with short and long referring to the clock-rate. The simulation results for the secret key fraction  $S(\Delta t, t_c)$  are presented in a two-dimensional parameter space in Fig. 5, assuming an ideal single-photon source ( $g^{(2)}(0) = 0$ ). In

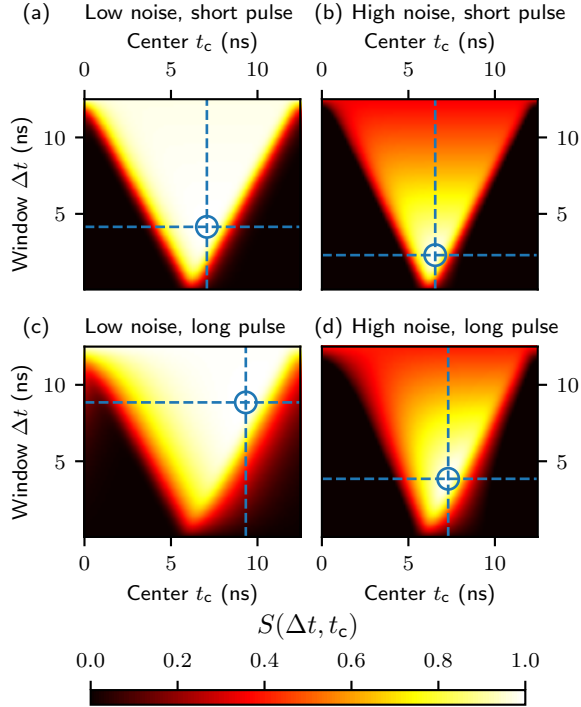


FIG. 5. Simulated back-to-back secret key rates achievable via temporal filtering for different pulse lengths and noise levels: (a) Low noise and long pulse (b) high noise and short pulse (c) low noise and long pulse, as well as (d) high noise and long pulse. Careful adjustment of the acceptance time windows results in a maximum in the secret key (see markers).

all four cases the temporal filtering enables one to find an optimal trade-off between sifted-key and QBER. Hence the secret key rate can be maximized by correctly choosing the settings of the temporal filter, resulting in a performance optimization of the QKD system. The gain in secret key rate compared to the case without applying a temporal filter is 2.5% in case (1), 184.5% in case (2), 6.0% in case (3), and 248.3% in case (4). Substantial improvements are achieved in the cases with high noise levels ((2) and (4)), corresponding to the regime of high transmission channel losses. Therefore, the optimization via temporal filtering becomes particular important in long distance QKD with noisy detectors. Using state-of-the-art superconducting single-photon detectors [37], the noise can be drastically reduced [38]. Many practical QKD scenarios, however, will not be able to provide the infrastructure for liquid-helium or closed-cycle refrigerators required for these detectors to date.

## DISCUSSION

We have demonstrated that temporal filtering of single-photon pulses is a viable tool to optimize the performance of QKD implementations based on sub-Poissonian quantum light sources. Using a basic QKD testbed comprising a solid-state based triggered SPS and a receiver module for four-state polarization coding, we showed that carefully setting the acceptance time windows enables one to maximize the achievable back-to-back secure key rate or the maximally tolerable transmission loss inside the quantum channel. Our optimization routine is particular beneficial in the high loss regime characteristic for long distance QKD. Additionally, we showed real-time security monitoring by evaluating the photon statistics of our SPS in terms of  $g^{(2)}(0)$  during the key generation.

The routines developed in our work with a basic BB84-QKD testbed are readily applicable for various implementations of quantum communication employing realistic quantum light sources, including measurement device-independent QKD and quantum repeaters, and are useful for certification of QKD [39]. Furthermore, the temporal filtering and real-time monitoring of sub-Poissonian light pulses opens up new possibilities for improving the performance taking detection flaws into account. Using SPSs for QKD, an attacker is forced to use a SPS as well. This in turn reduces the penalty on the achievable secret key rate taking detection flaws into account [40]. Even advanced non-linear attacks influencing or even controlling the photon statistics inside the quantum channel can be detected, by additionally monitoring  $g^{(2)}(0)$  on Alice' side. With respect to full implementations of QKD, further extensions are required, taking side-channel attacks [24, 41] or finite-key effects [42] into account. As the temporal filtering reduces the amount of key material that can be generated, finite-key size effects are getting increasingly important.

## METHODS

### Single-Photon Source

The SPS on Alice' side comprises a single pre-selected InGaAs/GaAs QD embedded in a monolithic microlens above a bottom distributed Bragg reflector, both of which increase the photon collection efficiency from the QD. Details on the sample and its deterministic fabrication can be found elsewhere [26, 43]. The SPS was mounted into a closed-cycle refrigerator integrated in a cryooptical table (Model attoDRY800, attocube systems AG) for operating the SPS at a temperature of 4.2 K. An aspheric lens ( $NA = 0.77$ ) inside the cryostat collected the QD emission, which was optically triggered at 80 MHz repetition rate using quasi-resonant excitation into the QD's

p-shell via a pulsed (2 ps pulse width) tunable laser system (picoEmerald, APE GmbH). Single-photon emission from the QD was spectrally filtered via an edge-pass filter and a monochromator coupled to a polarization maintaining single-mode fiber (PM 98-U25D) connected to the receiver module Bob. Here, the polarization of the single-photon pulses is set using a high-extinction-ratio linear-film polarizer followed by a lambda-half waveplate for aligning Alice' and Bob's polarization axes.

### Receiver Module Bob

The receiver module Bob contains a four-state polarization analyzer with passive basis choice. Here, the stream of single-photon pulses is split by a non-polarizing 50:50 beamsplitter (BS) followed by a polarizing beamsplitter (PBS) in the first output and a lambda-half waveplate combined with another PBS in the second output. Thus the four BB84 states (H-, V-, D-, and A-polarized photons) are routed in four different output ports, each comprising a fiber-collimator with attached optical multimode fiber (FG050LGA, Thorlabs GmbH). The photons are detected using four single-photon counting modules (COUNT-T100-FC, Laser Components GmbH) with a timing jitter between 500 ps and 600 ps. The single-photon detection events are converted to four streams of time tags (1 ps digital resolution) using a time-to-digital converter (TDC) (quTag, qutools GmbH) synchronized to the excitation laser.

### Postprocessing

To process the timetags from the receiver module, a homemade software package was developed (based on LabVIEW and Rust), in order to extract the sifted key fraction, the QBER, and the antibunching value  $g^{(2)}(0)$  as explained in the following. First, temporally filtered data sets were processed from the raw timetags by discarding events outside the specified acceptance time windows of width  $\Delta t$  and center  $t_t$ . For this purpose, slight temporal delays within Bob had to be compensated using electronic delays build in the TDC electronics. Afterwards the parameters mentioned above were extracted from the temporally filtered data sets. The QBER was calculated from the photon arrival time distributions as well as the sifted key. The photon statistics  $g^{(2)}(\tau)$  were evaluated in a  $\Delta\tau = 250$  ns-wide delay window, by correlating the timetags from the four detection channels of Bob. From the resulting  $g^{(2)}(\tau)$  histograms,  $g^{(2)}(0)$  was calculated via  $g^{(2)}(0) = \frac{A_{\tau=0}}{A_{\tau \neq 0}}$ , where  $A_{\tau=0}$  denotes the integrated area of the peak at zero time delay and  $A_{\tau \neq 0}$  the average area of the side peaks. The standard error of  $g^{(2)}(0)$  is deduced via Gaussian error propagation, taking into account  $\sigma(A_{\tau=0}) = \sqrt{A_{\tau=0}}$  as well as

the standard deviation of the areas from the side peaks. For illustrations in this work, a time-bin width of 25 ps and 250 ps were chosen for the photon arrival time distributions and  $g^{(2)}(\tau)$  histograms, respectively.

### Simulations

For the simulations the photon arrival time distributions of the single-photon pulses were modeled with synthetic pulse shapes using an exponential decay convoluted with a Gaussian of 500 ps FWHM, accounting for the temporal response function of the detection apparatus. Two types of QD-SPSs are considered: The first one resembles an QD with a radiative lifetime of 1.5 ns (long pulse) and the second one with a lifetime of 0.5 ns (short pulse). The optical imperfections in the second channel were modeled by the same distribution scaled to 1 %. The finite signal-to-noise-ratio (noise level) was considered by an uncorrelated offset of 0.01 per bin for low noise and 0.3 per bin for high noise, corresponding to signal-to-noise ratios of 392 and 13 in the input polarization channel. To account for effects arising from the overlap of consecutive pulses, a temporal window of 12.5 ns width was used from a train of three consecutive pulses.

The expected loss-dependent secret key in Fig. 3 (b) was calculated via Eq. 3 using estimated parameters extracted from our measurement data (see Supplementary Note 2). Cumulative detector dark counts of 100 Hz without temporal filtering were considered, leading to  $p_{dc} = 1.2 \cdot 10^{-6}$ . The mean photon number was estimated from the setup efficiency to be  $\mu \approx 0.0043$ .

### DATA AVAILABILITY

The data that support the plots within this paper and other findings of this study are available from the corresponding author upon reasonable request.

### ACKNOWLEDGMENTS

We acknowledge financial support from the German Federal Ministry of Education and Research (BMBF) via the project QuSecure (Grant No. 13N14876) within the funding program Photonic Research Germany and the German Research Foundation (DFG) via SFB 787 'Semiconductor Nanophotonics: Materials, Models, Devices'.

### AUTHOR CONTRIBUTIONS

T.K. designed and built the receiver module and the software used for the experiments. T.K. and M.v.H. run

the single-photon source, which was grown by J.-H.S. and A.S. and processed by M.G. and S.R. under supervision of S.R.. T.K. performed the experiments and analyzed the data, with input of L.R. and T.H.. T.K. and T.H. wrote the manuscript with input from all authors. T.H. conceived the experiment and supervised the project.

\* Corresponding author: [tobias.heindel@tu-berlin.de](mailto:tobias.heindel@tu-berlin.de)

[1] A. Acín, I. Bloch, H. Buhrman, T. Calarco, C. Eichler, J. Eisert, D. Esteve, N. Gisin, S. J. Glaser, F. Jelezko, S. Kuhr, M. Lewenstein, M. F. Riedel, P. O. Schmidt, R. Thew, A. Wallraff, I. Walmsley, and F. K. Wilhelm, *New J. Phys.* **20**, 080201 (2018).

[2] N. Gisin, G. Ribordy, W. Tittel, and H. Zbinden, *Rev. Mod. Phys.* **74**, 145 (2002).

[3] H.-K. Lo, M. Curty, and K. Tamaki, *Nat. Photon.* **8**, 595 (2014).

[4] E. Diamanti, H.-K. Lo, B. Qi, and Z. Yuan, *npj Quantum Inf.* **2**, 16025 (2016).

[5] C. H. Bennett and G. Brassard, Proceedings of IEEE International Conference on Computers, Systems and Signal Processing, Bangalore, India , 175 (1984).

[6] A. K. Ekert, *Phys. Rev. Lett.* **67**, 661 (1991).

[7] X.-B. Wang, *Phys. Rev. Lett.* **94**, 230503 (2005).

[8] A. Schlehahn, M. Gaafar, M. Vaupel, M. Gschrey, P. Schnauber, J.-H. Schulze, S. Rodt, A. Strittmatter, W. Stolz, A. Rahimi-Iman, T. Heindel, M. Koch, and S. Reitzenstein, *App. Phys. Lett.* **107**, 041105 (2015).

[9] F. Hargart, C. A. Kessler, T. Schwarzbäck, E. Koroknay, S. Weidenfeld, M. Jetter, and P. Michler, *App. Phys. Lett.* **102**, 011126 (2013).

[10] A. Schlehahn, A. Thoma, P. Munnelly, M. Kamp, S. Höfling, T. Heindel, C. Schneider, and S. Reitzenstein, *APL Photonics* **1**, 011301 (2016), <http://dx.doi.org/10.1063/1.4939831>.

[11] N. Somaschi, V. Giesz, L. De Santis, J. C. Loredo, M. P. Almeida, G. Hornecker, S. L. Portalupi, T. Grange, C. Antón, J. Demory, C. Gómez, I. Sagnes, N. D. Lanzillotti-Kimura, A. Lemaître, A. Auffeves, A. G. White, L. Lanco, and P. Senellart, *Nat. Photon.* (2016), 10.1038/nphoton.2016.23.

[12] H. Wang, Z.-C. Duan, Y.-H. Li, S. Chen, J.-P. Li, Y.-M. He, M.-C. Chen, Y. He, X. Ding, C.-Z. Peng, and et al., *Phys. Rev. Lett.* **116** (2016), 10.1103/physrevlett.116.213601.

[13] T. Heindel, C. Schneider, M. Lermer, S. H. Kwon, T. Braun, S. Reitzenstein, S. Höfling, M. Kamp, and A. Forchel, *App. Phys. Lett.* **96**, 011107 (2010).

[14] H. Wang, H. Hu, T.-H. Chung, J. Qin, X. Yang, J.-P. Li, R.-Z. Liu, H.-S. Zhong, Y.-M. He, X. Ding, Y.-H. Deng, Q. Dai, Y.-H. Huo, S. Höfling, C.-Y. Lu, and J.-W. Pan, *Phys. Rev. Lett.* **122** (2019), 10.1103/physrevlett.122.113602.

[15] L. Schweickert, K. D. Jöns, K. D. Zeuner, S. F. Covre da Silva, H. Huang, T. Lettner, M. Reindl, J. Zichi, R. Trotta, A. Rastelli, and V. Zwiller, *App. Phys. Lett.* **112**, 093106 (2018), <https://doi.org/10.1063/1.5020038>.

[16] L. Hanschke, K. A. Fischer, S. Appel, D. Lukin, J. Wierzbowski, S. Sun, R. Trivedi, J. Vučković, J. J. Finley, and K. Müller, *npj Quantum Inf.* **4** (2018), 10.1038/s41534-018-0092-0.

[17] E. Waks, K. Inoue, C. Santori, D. Fattal, J. Vuckovic, G. S. Solomon, and Y. Yamamoto, *Nature* **420**, 762 (2002).

[18] A. Beveratos, R. Brouri, T. Gacoin, A. Villing, J.-P. Poizat, and P. Grangier, *Phys. Rev. Lett.* **89**, 187901 (2002).

[19] R. Allaume, F. Treussart, G. Messin, Y. Dumeige, J.-F. Roch, A. Beveratos, R. Brouri-Tualle, J.-P. Poizat, and P. Grangier, *New J. Phys.* **6**, 92 (2004).

[20] P. M. Intallura, M. B. Ward, O. Z. Karimov, Z. L. Yuan, P. See, A. J. Shields, P. Atkinson, and D. A. Ritchie, *App. Phys. Lett.* **91**, 161103 (2007).

[21] R. J. Collins, P. J. Clarke, V. Fernández, K. J. Gordon, M. N. Makhonin, J. A. Timpson, A. Tahraoui, M. Hopkinson, A. M. Fox, M. S. Skolnick, and G. S. Buller, *J. Appl. Phys.* **107**, 073102 (2010).

[22] K. Takemoto, Y. Nambu, T. Miyazawa, K. Wakui, S. Hirose, T. Usuki, M. Takatsu, N. Yokoyama, K. Yoshino, A. Tomita, S. Yorozu, Y. Sakuma, and Y. Arakawa, *App. Phys. Express* **3**, 092802 (2010).

[23] T. Heindel, C. A. Kessler, M. Rau, C. Schneider, M. Fürst, F. Hargart, W.-M. Schulz, M. Eichfelder, R. Robach, S. Nauerth, M. Lermer, H. Weier, M. Jetter, M. Kamp, S. Reitzenstein, S. Höfling, P. Michler, H. Weinfurter, and A. Forchel, *New J. Phys.* **14**, 083001 (2012).

[24] M. Rau, T. Heindel, S. Unsleber, T. Braun, J. Fischer, S. Frick, S. Nauerth, C. Schneider, G. Vest, S. Reitzenstein, M. Kamp, A. Forchel, S. Höfling, and H. Weinfurter, *New J. Phys.* **16**, 043003 (2014).

[25] E. Waks, C. Santori, and Y. Yamamoto, *Phys. Rev. A* **66**, 042315 (2002).

[26] M. Gschrey, A. Thoma, P. Schnauber, M. Seifried, R. Schmidt, B. Wohlfeil, L. Krüger, J. H. Schulze, T. Heindel, S. Burger, F. Schmidt, A. Strittmatter, S. Rodt, and S. Reitzenstein, *Nat. Commun.* **6** (2015), 10.1038/ncomms8662.

[27] H. Ko, K.-J. Kim, J.-S. Choe, B.-S. Choi, J.-H. Kim, Y. Baek, and C. J. Youn, *Sci. Rep.* **8** (2018), 10.1038/s41598-018-33699-y.

[28] E. Schöll, L. Hanschke, L. Schweickert, K. D. Zeuner, M. Reindl, S. F. C. da Silva, T. Lettner, R. Trotta, J. J. Finley, K. Müller, A. Rastelli, V. Zwiller, and K. D. Jöns, *Nano Lett.* **19**, 2404 (2019).

[29] A. W. Schell, J. Kaschke, J. Fischer, R. Henze, J. Wolters, M. Wegener, and O. Benson, *Sci. Rep.* **3**, (2013).

[30] R. Brouri, A. Beveratos, J.-P. Poizat, and P. Grangier, *Opt. Lett.* **25**, 1294 (2000).

[31] C. Becher, A. Kiraz, P. Michler, A. Imamoglu, W. V. Schoenfeld, P. M. Petroff, L. Zhang, and E. Hu, *Phys. Rev. B* **63**, 121312 (2001).

[32] H. Kumano, T. Harada, I. Suemune, H. Nakajima, T. Kuroda, T. Mano, K. Sakoda, S. Odashima, and H. Sasakura, *App. Phys. Express* **9**, 032801 (2016).

[33] H.-K. Lo, M. Curty, and B. Qi, *Phys. Rev. Lett.* **108** (2012), 10.1103/physrevlett.108.130503.

[34] V. V. Kuzmin, D. V. Vasilyev, N. Sangouard, W. Dr, and C. A. Muschik, arXiv preprint arXiv:1905.00335 (2019).

[35] J. F. Dynes, M. Lucamarini, K. A. Patel, A. W. Sharpe, M. B. Ward, Z. L. Yuan, and A. J. Shields, *Opt. Express* **26**, 22733 (2018).

- [36] M. Kumazawa, T. Sasaki, and M. Koashi, *Opt. Express* **27**, 5297 (2019).
- [37] I. E. Zadeh, J. W. N. Los, R. B. M. Gourgues, V. Steinmetz, G. Bulgarini, S. M. Dobrovolskiy, V. Zwiller, and S. N. Dorenbos, *APL Photonics* **2**, 111301 (2017).
- [38] A. Boaron, G. Boso, D. Rusca, C. Vulliez, C. Autebert, M. Caloz, M. Perrenoud, G. Gras, F. Bussières, M.-J. Li, D. Nolan, A. Martin, and H. Zbinden, *Phys. Rev. Lett.* **121** (2018), 10.1103/physrevlett.121.190502.
- [39] A. Tomita, *Adv. Quantum Technol.* **2**, 1900005 (2019).
- [40] L. Lydersen and J. Skaar, *Quantum Inf. Comput.* **10**, 60 (2010).
- [41] S. Sajeed, P. Chaiwongkhot, J.-P. Bourgoin, T. Jennewein, N. Lütkenhaus, and V. Makarov, *Phys. Rev. A* **91** (2015), 10.1103/physreva.91.062301.
- [42] V. Scarani, H. Bechmann-Pasquinucci, N. J. Cerf, M. Dušek, N. Lütkenhaus, and M. Peev, *Rev. Mod. Phys.* **81**, 1301 (2009).
- [43] T. Heindel, S. Rodt, and S. Reitzenstein, “Single-photon sources based on deterministic quantum-dot microlenses,” in *Quantum Dots for Quantum Information Technologies*, edited by P. Michler (Springer International Publishing, Cham, 2017) pp. 199–232.

## SUPPLEMENTARY INFORMATION

**Note 1: Measurement data for QBER and signal fraction for each polarization**

The most simple temporal filter comprises an acceptance time window centered at the maximum of the photon arrival time distribution. For light sources with a symmetric distribution this is sufficient. For the asymmetric temporal shape of quantum emitters, arising from their spontaneous radiative decay, however, this is not sufficient (see Supplementary Note 3).

From the photon arrival time distributions of Fig. 1 (d) in the main text the QBER for all four possible input polarizations is calculated (see Fig. S1). Reducing the size of the acceptance time window, we expect a decrease in QBER due to the improvement in signal-to-noise ratio. This is observed for the V and A polarization. The minimum QBER is achieved at  $\Delta t = 0.2$  ns and  $\Delta t = 0.05$  ns, respectively. The slope is correlated to the shape of photon arrival time distribution. The measurement for the H polarization shows a slightly different behavior. Here, a local minimum at  $\Delta t = 1.7$  ns is observed. This discrepancy most probably arises from the fact, that the four single-photon detectors used in our experiments slightly differ in their properties (e.g. temporal jitter), which needs to be taken into account in the security analysis in full implementations of QKD. Another discrepancy is observed for the D input polarization. The minimal achievable value  $QBER_D$  is reached for an acceptance window of  $\Delta t = 5.3$  ns. In addition, the low extinction ratio in reflection of the polarizing beam splitter in the D/A-basis leads to a high QBER.

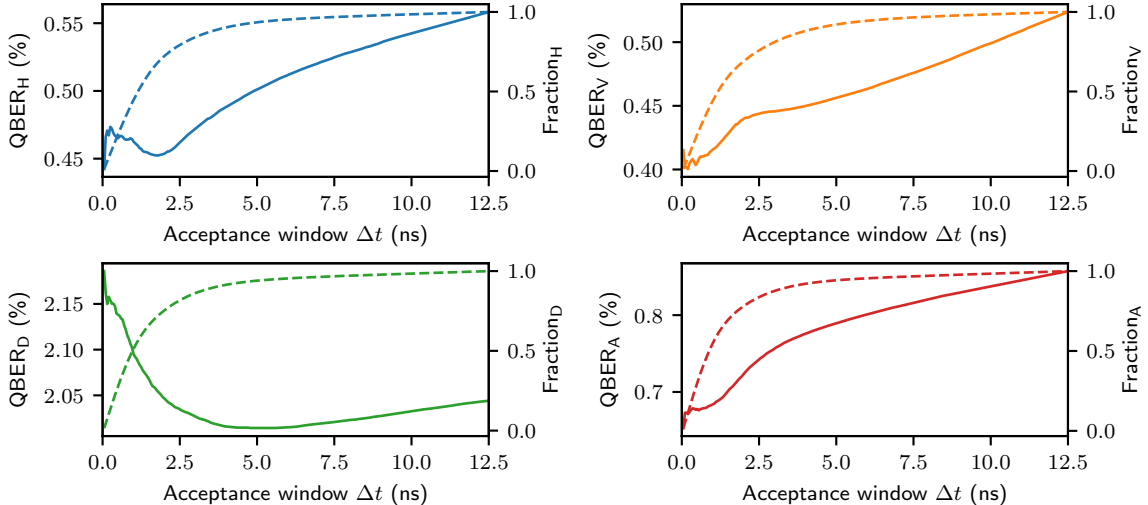


FIG. S1. The effect of temporal filtering on the QBER and Fraction of the overall signal for each polarization.

**Note 2: Parameter estimation for calculating the expected secret key rates**

The expected key rates  $R$  in Fig. 3 (b) in the main text are calculated from equation of [25]:

$$R = \frac{p_{\text{click}}}{2} (\beta\tau(e) - f(e)h(e)). \quad (4)$$

with the binary Shannon entropy  $h(e) = -e\log_2(e) - (1-e)\log_2(1-e)$ . The parameters used for the calculation stem from the long-term measurement for fixed  $H$  input polarization. The extraction from this data is described in the following for the mean photon number  $\mu$ , the detection rate  $p_{\text{click}}$  and detector dark count probability  $p_{\text{dc}}$ . The parameters are summarized in Table S1. The mean photon number  $\mu$  at Alice's output was calculated from the clock frequency of the excitation laser (80 MHz), the setup efficiency and the mean detector count rate on all four detectors during the measurement. This results a mean photon number  $\mu = 0.0043$ . This already low value does not allow for further optimization of  $\mu$  as in [25]. The detector dark counts can be estimated by two ways. Shielding the detectors from all incoming light results in a cumulative dark count rate of below 100 Hz. For taking into account the

Relevant parameter	Symbol	Value
Mean Photon number	$\mu$	0.0043
Dark count probability	$p_{dc}$	$1.22 \cdot 10^{-6}$

TABLE S1. Parameters for the estimation of the expected secret key rates.

detectors breakdown flash and reflection of the optics during the operation, a second method is implied to estimate the dark count rate in the laboratory environment. The events in the  $D$  channel are summed up in a region governed by noise and divided by the measurement time. This does also result in an overall dark count rate of 100Hz. For the acceptance window of 12.5 ns this leads to  $p_{dc} = 1.22 \cdot 10^{-6}$ .

**Note 3: Impact of 2D temporal filtering on the performance of single-photon QKD**

For signal pulses which are asymmetric in the temporal domain, the acceptance time-windows for QKD need to be adjusted in two dimensions using its width  $\Delta t$  and its center position  $t_c$ . In Figure 3(a) of the main text, we present the secret key rate  $S(\Delta t, t_c)$  in this 2D parameter space. Supplementary Figure S2 depicts the complementing data for the signal fraction, the QBER, the  $g^{(2)}(0)$ , and the resulting secret key rate.

**Note 4: Impact of temporal filtering on the achievable communication distance**

As mentioned in the discussion of Figure 3(b), temporal filtering can be exploited to enhance the signal-to-noise ratio resulting in enhanced tolerable losses in single-photon QKD. Figure S3 for clarity depicts the tolerable losses, the QBER, and  $g^{(2)}(0)$  as a function of the width  $\Delta t$  of the acceptance time window (at fixed center position  $\Delta t = 6.25$  ns).

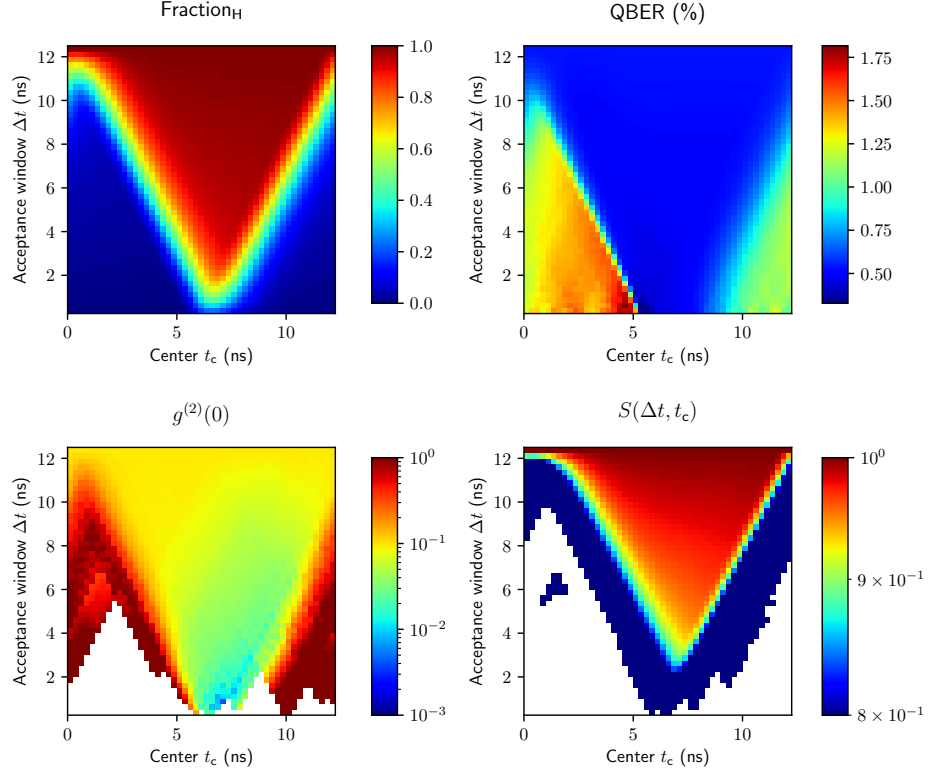


FIG. S2. The effect of 2D temporal filtering on key parameters of QKD: Fraction of signal, QBER,  $g^{(2)}(0)$ , and therefrom estimated secret key rate for realistic-SPS from Eq. (4). The white regions in the  $g^{(2)}(0)$  parameter map indicate parameters where the autocorrelation could not be evaluated. The white regions in the secret key rate map indicate parameters for which no secret key can be extracted.

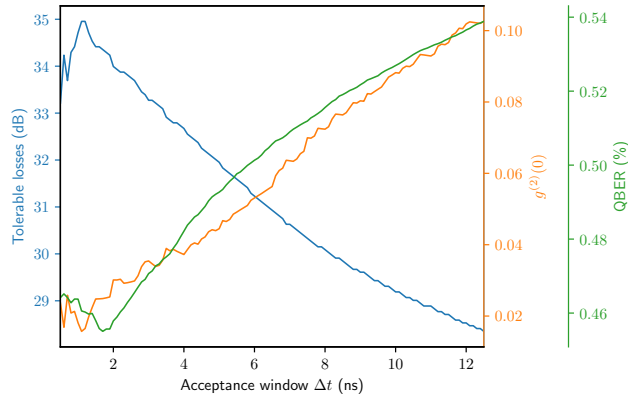


FIG. S3. Effect of temporal filtering on the tolerable loss in single-photon QKD (for fixed  $t_c = 6.25$  ns). Reducing the acceptance time window's width  $\Delta t$  results in an enhanced signal-to-noise ratio as indicated by improved QBER and  $g^{(2)}(0)$ . This leads to enhancement of the tolerable loss and therefore to an extension of the achievable communication distance.